Science of the Total Environment 826 (2022) 153915

Contents lists available at ScienceDirect

Science of the Total Environment

journal homepage: www.elsevier.com/locate/scitotenv

# Phenotypic and transcriptional study of the antimicrobial activity of silver and zinc oxide nanoparticles on a wastewater biofilm-forming *Pseudomonas aeruginosa* strain

M. de Celis, I. Belda, D. Marquina, A. Santos *

*Department of Genetics, Physiology and Microbiology, Microbiology Unit, Faculty of Biology, Complutense University of Madrid, José Antonio Novais 12, 28040 Madrid, Spain*

## HIGHLIGHTS

- Biofilm formation is a defensive mechanism against metal NPs.
- Metal NPs induce an iron homeostasis-related transcriptomic response.
- WWTP-isolated *P. aeruginosa* strain resist high concentrations of Ag NPs.
- ZnO NPs increased eDNA release via cell death induced by ROS production.

## GRAPHICAL ABSTRACT

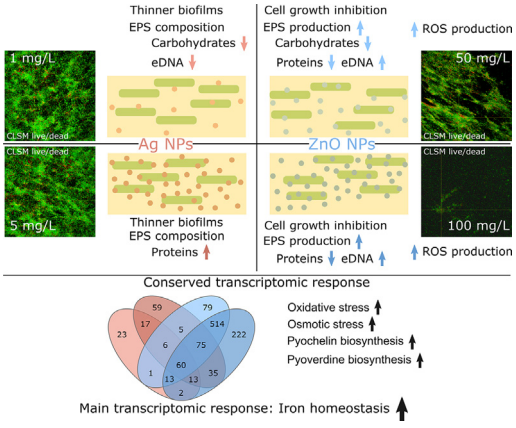


## ARTICLE INFO

*Article history:*
Received 14 October 2021
Received in revised form 11 February 2022
Accepted 12 February 2022
Available online 24 February 2022

Editor: Damia Barcelo

*Keywords:*
Zinc oxide nanoparticles
Silver nanoparticles
*Pseudomonas aeruginosa*
*Biofilm*
RNA-seq
Transcriptional responses

## ABSTRACT

The extensive use of nanoparticles (NPs) in industrial processes makes their potential release into the environment an issue of concern. Ag and ZnO NPs are among the most frequently used NPs, potentially reaching concentrations of 1–4 and 64 mg/kg, respectively, in Wastewater Treatment Plants (WWTPs), with unknown effects over microbial populations. Thus, we examined, in depth, the effect of such NPs on a *P. aeruginosa* strain isolated from a WWTP. We evaluated the growth, ROS production and biofilm formation, in addition to the transcriptomic response in presence of Ag and ZnO NPs at concentrations potentially found in sewage sludge. The transcriptomic and phenotypic patterns of *P. aeruginosa* in presence of Ag NPs were, in general, similar to the control treatment, with some specific transcriptional impacts affecting processes involved in biofilm formation and iron homeostasis. The biofilms formed under Ag NPs treatment were, on average, thinner and more homogeneous. ZnO NPs also alters the biofilm formation and iron homeostasis in *P. aeruginosa*, however, the higher and more toxic concentrations utilized caused an increase in cell death and eDNA release. Thus, the biofilm development was characterized by EPS production, via eDNA release. The number of differentially expressed genes in presence of ZnO NPs was higher compared to Ag NPs treatment. Even though the responses of *P. aeruginosa* to the presence of the studied metallic NPs was at some extent similar, the higher and more toxic concentrations of ZnO NPs produced greater changes concerning cell viability and ROS production, causing disruption in biofilm development.

* Corresponding author.
*E-mail address:* ansantos@ucm.es (A. Santos).

http://dx.doi.org/10.1016/j.scitotenv.2022.153915

## 1. Introduction

Nanoproducts and nanomaterials with novel physical and chemical properties, such as increased surface area and reactivity, have been widely applied in areas such as medicine, cosmetic, or textile (Fabrega et al., 2011). Because of their extensive use, the occurrence of nanoparticles (NPs) in the environment has become an issue of concern. Silver (Ag) and zinc oxide (ZnO) are among the most frequently used NPs, and thus, their potential release into waste streams poses a risk to environmental and human health (Ma et al., 2013; Sikder et al., 2017). One of the main ways for metallic NPs to reach the environment is through wastewater treatment plants (WWTPs), where NPs tend to accumulate in the sludge (Durenkamp et al., 2016). The performance of wastewater treatment relies in activated sludge processes, and hence, the presence of toxic levels of NPs in these systems is likely to have adverse effects on the activity and structure of resident microbial communities (Brar et al., 2010; Gwin et al., 2018). Previous studies have reported concentrations of Ag NPs in environmental systems in the range of 0.01 ng/L to 10 μg/L (Gottschalk et al., 2013). However, their Predicted Environmental Concentrations (PECs) of Ag NPs in sewage sludge rise to 1–4 mg/kg levels (Gottschalk et al., 2009). Besides, the predicted concentration of ZnO NPs ranges from 1 to 100 ng/L in rivers and wastewaters to 100 mg/kg measured in soil (Jones et al., 2008). However, PECs in sewage sludge reach up to 64.7 mg/kg (Majedi et al., 2012).

The toxicity and antimicrobial effect of Ag and ZnO nanoparticles is attributed to numerous factors and is dependent of factors like particle size, concentration, and surface charge (Silva et al., 2014). Ag NPs are often used as antimicrobial agents in a wide variety of products. This toxicity is the result of the combination of various simultaneous effects on bacterial cells, hindering their adaptation and defense against Ag NPs presence (Slavin et al., 2017). Among these effects, the release of silver ions through particle oxidation has been discussed (Zhang et al., 2011). These ions can damage several functions of the bacterial cell, through forming bonds with functional groups that contain sulfur (Lalley et al., 2014). The exposure of Ag NPs to oxygen also produces Reactive Oxygen Species (ROS), oxidizing important bacterial cellular components (Fauss et al., 2014). On the other hand, the exact mechanism of action of ZnO NPs against bacterial cells is still not clear, however, their role in the generation of ROS is thought to be the main cause of their antimicrobial activity (Pati et al., 2014; da Silva et al., 2019). Besides, the release of toxic levels of $Zn^{2+}$ has been proposed as another major cause of their cytotoxicity (Ivask et al., 2014). In addition, interactions between ZnO NPs with the cell wall and intracellular components lead to interrupted bacterial growth, cellular surface abrasiveness and cell wall deformation (Ahmed et al., 2019).

The biocide activity of nanomaterials can be exploited for numerous applications, but most research on this topic focuses on toxicity against specific bacterial strains, in the search of new tools against bacterial infections (Liao et al., 2019). Another studied application that intends to use the antimicrobial activity of NPs is to enhance the performance of conventional filtration membranes at the industrial scale, by improving the prevention of biological fouling (Liu et al., 2017; Beisl et al., 2019). Similar efforts have been put on developing enzymatic approaches to minimize the colonization and growth of microorganisms in filtration membranes (de Celis et al., 2021).

Bacteria colonize surfaces, such as industrial filtration membranes or implanted medical devices, by forming biofilms, growing in aggregates embedded in a matrix of Extracellular Polymeric Substances (EPS) (West et al., 2006). These biofilms provide bacteria multiple advantages such as structural stability or protection and increased access to nutrients, representing an essential mechanism of colonization in many natural and anthropic systems (Huang et al., 2019). In addition to an improved resistance against traditional antimicrobial agents (i.e., antibiotics), biofilm formation allows the bacterial cells to escape the immune response of the host, whose immune system is not able to eliminate the pathogen, but instead increase collateral tissue damage (Vestby et al., 2020). Currently, there is a myriad of methods targeting biofilms for therapeutics against bacterial infections, like phytochemicals, bacteriophage therapy, antimicrobial peptides, or nanoparticle treatment (Sharma et al., 2014).

*Pseudomonas aeruginosa* is a ubiquitous Gram-negative bacterium, that is one of the most common causes of opportunistic human infections, and which is found in water systems, like WWTPs (Slekovec et al., 2012). Biofilm formation in *P. aeruginosa* is regulated by Quorum Sensing (QS) systems, that controls the behavior of diverse bioactivities, metabolic pathways, and stress responses compared to planktonic cells (Klausen et al., 2003). Nowadays, there is a knowledge gap concerning the gene responses triggered by the influence of metallic NPs and their effect on bacterial features controlled by QS, like biofilm formation (Gómez-Gómez et al., 2019a).

In this context, we examined the effect of Ag and ZnO NPs in a biofilm-forming *P. aeruginosa* strain isolated from a WWTP. In this work we examined the biofilm inhibition activity and the potential danger of PECs of Ag and ZnO NPs in bioreactors of WWTP, using a *P. aeruginosa* strain. We assessed the antimicrobial effects of NPs at concentrations potentially found in sewage sludge, evaluating the growth and biofilm formation capabilities of *P. aeruginosa*. Besides, we evaluated the production of ROS and the structural characteristics, as well as matrix composition, of matured biofilms exposed to NPs. Finally, we conducted a transcriptomic study to gain insight into the changes in gene expression produced by the impact of Ag and ZnO NPs at PEC concentrations in *P. aeruginosa*.

## 2. Material and methods

### 2.1. ZnO and Ag nanoparticles

ZnO NPs aqueous dispersion was purchased from Sigma-Aldrich, and Ag NPs coated in citrate and of 20 nm size were obtained as an aqueous dispersion from Nanocomposix™ (Nanocomposix). The desired concentrations of NPs were obtained by diluting NPs dispersions in sterile Milli-Q water and sonicated 30 min in an ultrasonic bath prior use. A full description of the NPs preparations used, and their physical-chemical characterization were done by Gómez-Gómez et al. (2019a) and are represented in Table S1. Considering that the characterization of NPs made in this study was in standard conditions, for further studies assessing the NP-*P. aeruginosa* cells interactions additional NP characterization should be made in the experimental conditions used in this study. The used NPs are mostly aggregated (Fig. S1); however, no prevention of aggregation was applied since NPs tend to be aggregated in the environment (Hotze et al., 2010). We tested broad concentrations of Ag and ZnO NPs (Fig. S2) however, we selected two environmentally relevant concentrations, as revealed by the modeling studies (Jones et al., 2008; Gottschalk et al., 2009; Majedi et al., 2012).

### 2.2. Bacterial strain and growth conditions

The *P. aeruginosa* M3.15R2 strain used in this study was isolated from a full-scale MBR-WWTP described elsewhere (de Celis et al., 2020). *P. aeruginosa* was grown at 28 °C in Luria-Bertani Broth (LB) medium prepared with potassium phosphate buffer 0.1 M pH 6.5, to compare the potential biofilm inhibition effectiveness of the NPs selected in this study (Ag and ZnO NPs) with acylase enzymes (de Celis et al., 2021).

### 2.3. Effect of Ag and ZnO nanoparticles on the viability and ROS formation in P. aeruginosa

*P. aeruginosa* was inoculated at 0.01 $OD_{600nm}$ in LB medium in absence and presence of Ag (1 and 5 mg/L) and ZnO (50 and 100 mg/L) NPs. LB medium was buffered (phosphate buffer 0.1 M) to prevent pH changes. Cultures were incubated for 24 h at 28 °C and 120 rpm shaking. Then, an aliquot of each culture was serially diluted and spread on LB-agar plates to determine the number of Colony Forming Units (CFU) per milliliter. Besides, the same experiment was repeated measuring $OD_{600nm}$ every hour using a microplate reader (Varioskan Flash Multimode Reader, Thermo

Scientific, USA). Growth curves were further analyzed using the growthrates R package (Petzoldt, 2017) to find the maximum growth rate and the carrying capacity of *P. aeruginosa*, the lag time was estimated calculating the intercept of the tangent to the growth curve with the x axis (Zwietering et al., 1990). Significant differences between NPs addition and control condition were studied using Student's *t*-test.

The intracellular ROS was measured using 2′,7′-dichlorodihydrofluorescein diacetate (DCFH-DA, Sigma-Aldrich, USA) following the procedure described by Gerber and Dubery (2003). Briefly, *P. aeruginosa* cultures in mid-exponential growth phase (5 h) were transferred to fresh LB medium and treated with 50 and 100 mg/L ZnO NPs, and 1 and 5 mg/L Ag NPs as the four experimental conditions or left untreated as the control condition. Then, 190 μL of cell suspensions were transferred to multiwell dishes and were incubated for 2 h in presence of 10 μL of DCFH-DA 1 mM. After entering the cells, intracellular esterases transform DCFH-DA into 2′, 7′-dichlorodihydrofluorescein (H2DCF) and latter converted to fluorescent 2′, 7′-dichlorofluorescein (DCF) by intracellular ROS. For intracellular ROS quantification the absorbance at 600 nm and the Fluorescence Intensity (FI), with excitation and emission wavelengths of 485 nm and 530 nm, respectively, were measured in a Varioskan Lux plate reader (Thermo Scientific, UK). Significant effect of NPs addition against control condition was studied using Student's *t*-test.

### 2.4. P. aeruginosa biofilm formation assays in Ag and ZnO NPs dispersions

Biofilm formation was assayed in 96-well plates following the method previously described by Merritt et al. (2005) with some modifications. Briefly *P. aeruginosa* suspensions (final $OD_{600}$ = 0.01) were incubated in absence or presence of Ag (1 and 5 mg/L) and ZnO (50 and 100 mg/L) NPs. Plates were incubated at 28 °C for 24 h without shaking. After removing medium and planktonic cells, wells were washed with distilled water and biofilm biomass stained for 15 min using a 0.1% (p/v) Crystal Violet (CV) solution. Unbound dye was removed by washing wells with distilled water and plates were air-dried before solubilizing CV with 30% (*v*/v) acetic acid. After 20 min of incubation, absorbance was measured at 570 nm in a Varioskan Lux plate reader.

Besides, *P. aeruginosa* suspensions, with and without adding the studied concentrations of NPs, were used for inoculating chamber slides (final $OD_{600}$ = 0.01) that were incubated at 28 °C for 24 h in a closed, humidified container. After the incubation, planktonic cells were washed, and the biofilm structure was studied by confocal laser scanning microscopy (CLSM). The slides were stained using LIVE/DEAD BacLight Bacterial Viability kit (Thermo Scientific, USA) with propidium iodide (PI) and SYTO9 to detect dead and live cells, respectively. Image acquisition was performed using a LEICA TCS SP8 STED 3× equipped with a 20× dry objective (Leica, Germany). For each image stack, roughness coefficient (indicator of biofilm heterogeneity), surface/biovolume ratio, surface area, cellular biomass and average thickness were calculated using COMSTAT (Heydorn et al., 2000). Significant differences between conditions were studied using ANOVA and Least Significant Difference (LSD) tests (a-c significance groups).

### 2.5. Extraction of biofilm extracellular matrix and quantification of eDNA, proteins and carbohydrates

Extracellular polymeric substances (EPS) of *P. aeruginosa* biofilms were extracted as previously described (Ouyang et al., 2020) with modifications. Briefly, we incubated *P. aeruginosa* in absence and presence of studied NPs in 12-wells culture plates and cultured for 24 h at 28 °C without shaking. Planktonic bacterial cells were washed with phosphate-buffered saline (PBS; VWR Life Sciences, Ohio), while biofilms were recovered by scrapping and resuspended in 1 mL PBS. Then, biofilm samples were vortexed for 1 min and then sonicated in an ultrasonic bath for 5 min, followed by another vortex step of 1 min. Lastly, we centrifuged the samples (3000 *g*; 10 min) and filtered the supernatant fraction through 0.2 μm PVFD filters. For dry weight calculations filters were weighted before and after biofilm filtration followed by drying at 60 °C, obtaining the difference between the two weight measures.

The major components of EPS in biofilm matrix are eDNA, proteins and carbohydrates, thus these substances were quantified. The amount of eDNA was determined measuring the absorbance at 260 nm of the extracted biofilm matrix, as it is the main nucleic acid present in the *P. aeruginosa* biofilm (Flemming and Wingender, 2010). The Bradford method, with modifications, was used for quantification of extracellular proteins present in biofilm matrix. Briefly, 50 μL of Bradford reagent was added to 150 μL of diluted biofilm matrix, incubated 5 min at room temperature and measured its absorbance at 595 nm using a plate reader (Varioskan Lux). Total carbohydrate content was determined based on the phenol–sulfuric acid method of Dubois et al. (1956). Although the phenol-sulfuric method is used to quantify neutral sugars, it is suitable to quantify the main polysaccharides conforming the EPS of *P. aeruginosa* biofilms (Jennings et al., 2015; Pestrak et al., 2018). Briefly, 200 μL of the isolated EPS were mixed with 1000 μL of sulfuric acid and then with 200 μL phenol 5% and incubated 10 min at room temperature. The absorbance of the mixture was measured at 490 nm. Total eDNA, protein and carbohydrate contents were expressed as a function of the dry weight of the biofilm (milligrams per gram of biofilm dry weight). Student's *t*-test was used to assess the significance of NP effect against control condition.

### 2.6. Transcriptomic response of P. aeruginosa to Ag and ZnO NPs

*P. aeruginosa* M3.15R2 strain was cultured in buffered LB for 17 h at 28 °C and 180 rpm in presence or absence of Ag and ZnO NPs at the studied concentrations. Cultures were then centrifuged at 1500 *g* for 10 min and biomass was immediately frozen at −80 °C until RNA extraction.

#### 2.6.1. RNA preparation and sequencing

RNA was extracted from frozen biomass using NZY total RNA isolation kit (NZYtech, Portugal). RNA quality analysis, library preparation and RNA sequencing were carried out at the Bioinformatics and Genomics Unit of The Institute of Parasitology and Biomedicine "López-Neyra" (IPBLN-CSIC, Granada, Spain). The quality of the RNAs was evaluated by Bioanalyzer (Agilent Technologies) and samples with RNA Integrity Number (RIN) ≥ 8.1 were selected to subsequent analysis. Next, rRNA was depleted using the NEBNext rRNA Depletion Kit (Bacteria; New England Biolab) following manufacturer's specifications. Finally, libraries were constructed using TruSeqTM Stranded RNA sample preparation Kit, according to Illumina's instructions. In addition, libraries quality was validated by Qubit dsDNA HS Assay Kit (Thermo Fisher) and 2100 Bioanalyzer (Agilent Technologies). Afterwards, these libraries were sequenced on an Illumina NextSeq 500, producing 30 Gbp of 75 bp paired end reads.

#### 2.6.2. Transcriptome data analysis

MiARma-Seq pipeline, with modifications, was used to analyze transcriptomic data (Andres-Leon et al., 2016). Briefly, quality evaluation of raw data was done using FastQC software (Andrews, 2010). We used sortmeRNA software to filter overrepresented rRNA fragments (Kopylova et al., 2012). Then, the resulting reads were mapped to *P. aeruginosa* PAO1 genome (GenBank accession code: ASM676v1.37) using Burrows-Wheeler Aligner (BWA) v0.7.11 (Li and Durbin, 2009), and the number of read counts per feature was obtained using Htseq-count v0.6.1 (Anders et al., 2015). Differently Expressed (DE) genes were calculated in comparisons between different treatments, using DESeq2 package v1.26.0 (Love et al., 2014). A gene is considered DE if the False Discovery Rate (FDR) value is <0.05. In order to envisage the effect of gene expression alteration in a broader way, Gene Ontology (GO) biological process enrichment was calculated from the locus gene name from *P. aeruginosa* previously acquired from GenBank.

## 3. Results and discussion

Currently, there is little concern in the environmental risk of nanomaterials, however, more attention should be paid to the risk in scenarios close to potential point sources such as sewage sludge or wastewater effluent (Zhao et al., 2021). The highest PECs, in the range of mg/kg, have been found in wastewater sludge (Sun et al., 2016), and their areas of discharge (Li et al., 2016; Wimmer et al., 2019). Bioaccumulation and biomagnification of nanomaterials in nature will make their toxic effects more evident, with the potential to affect all living organisms, making their misuse one of the biggest threats to the environment (Danabas et al., 2020). Thus, we studied the antimicrobial effect of Ag and ZnO NPs on a WWTP-isolated strain of *P. aeruginosa,* at concentrations (PECs) that are expected to be found in sewage sludge (Gottschalk et al., 2009; Majedi et al., 2012).

### 3.1. Antimicrobial effect of ZnO NPs and Ag NPs in P. aeruginosa

The antimicrobial effect of Ag and ZnO NPs was assessed measuring the cellular viability, the oxidative stress, and the biofilm formation ability of *P. aeruginosa* when treated with 1 and 5 mg/L of Ag NPs and, 50 and 100 mg/L of ZnO NPs. The cellular viability was studied measuring the cell count after 24 h incubation. In presence of Ag NPs there were no significant changes in cell viability, however, when exposed to 50 mg/L and 100 mg/L ZnO NPs the viability was decreased by 90% and 99.7%, respectively (Fig. 1A). Besides, growth curves of *P. aeruginosa* in presence of 50 and 100 mg/L ZnO NPs showed the lower growth rates and maximum density, compared to control and Ag NPs treated cultures (Fig. S3; Table S2). Although the studied concentrations of Ag NPs are considered within the toxic range for clinical isolates of *P. aeruginosa* (Habash et al., 2017), the WWTP-isolated strain used in our study seemed to show an increased resistance to Ag NPs possibly caused by a constant exposition to such NPs or similar toxic agents present in wastewater. Despite the increased lag time in presence of Ag NPs, growth rate and carrying capacity were not affected (Fig. S3; Table S2). The increase in lag phase has been described as a key strategy for bacteria to defend themselves from sub-inhibitory concentrations of Ag NPs (Guo et al., 2020). Thus, this strain could be more adapted to Ag NPs, and hence, be able to resist higher concentrations (Dhas et al., 2013), or this reduced toxic effect of Ag NPs could be explained by the effect of the assayed conditions which could affect speciation, inactivate, or precipitate Ag NPs reducing their toxicity. The oxidative stress production agreed with the cell viability results obtained, without significant changes in presence of Ag NPs but an increase in ROS production in presence of ZnO NPs. In presence of 100 mg/L of ZnO NPs the ROS production almost doubled compared to the control, whereas in presence of 50 mg/L it increased by close to 30% (Fig. 1B). Indeed, the cytotoxicity observed for ZnO NPs are attributed to the generation of ROS when they get in contact with bacterial cells (Chen et al., 2017). Lastly, we measured the biofilm development by CV staining. We observed higher levels of biofilm formation when *P. aeruginosa* grew in presence of all the studied NPs concentrations compared to control cultures (Fig. 1C). In particular, we found a greater increase in presence of 100 mg/L ZnO NPs, where the biofilm formation increased by approximately 250% compared to the control, doubling the increase produced in presence of the rest of the treatments. This increase in biofilm formation in presence of NPs, could be probably related to the greater stress tolerance that *P. aeruginosa* gets when growing on biofilms (Periasamy et al., 2015). In fact, we observed that, when the oxidative stress is higher and the cell viability lower, the biofilm biomass is also higher, responding to the stress in an attempt to survive in such harsh conditions. The stress produced by ZnO NPs could induce an eDNA release and EPS (Fig. 2), increasing the biofilm formation measured compared to the cell viability observed. It should be considered that biofilm formation was assessed by the CV method that stains both bacterial cells and EPS. At the studied concentrations ZnO NPs have higher toxicity to *P. aeruginosa* M315R2 than Ag NPs. In addition to the different NP concentration tested, ZnO NPs have higher magnitude of charge difference than Ag NPs with *P. aeruginosa* cells (Table S1), revealing higher attraction forces (Silva et al., 2014). This might represent increased physical contact between ZnO NPs and bacterial cells, leading to higher toxicity.

### 3.2. Effect of Ag and ZnO NPs on the composition and structure of biofilms of P. aeruginosa

To evaluate the effect of studied NPs on the biofilm matrix (EPS), the concentration of extracellular components of the biofilm matrix (i.e., eDNA, proteins, and carbohydrates) was quantified (Fig. 2). As significant changes compared to the control condition, the content of eDNA and carbohydrates in *P. aeruginosa* biofilm matrix decreased, on average, by 32.82% and 59.92%, after exposure to 1 mg/L Ag NPs, respectively, whereas protein content increased by 49.16% after exposure to 5 mg/L Ag NPs. On the other hand, the composition of the biofilm matrix in presence of ZnO NPs differed mainly on eDNA concentrations, giving 50 and 100 mg/L ZnO NPs a similar response of an overall average increase of 91.97% compared to the control condition. Protein concentration was decreased after exposure to ZnO NPs, again independently on the NPs concentration used, in a 62.04%, on average, compared to the control condition. Additionaly, after incubation with 50 mg/L ZnO NP, the concentration of carbohydrates decreased by 59.33%; however there is a notable dispersion

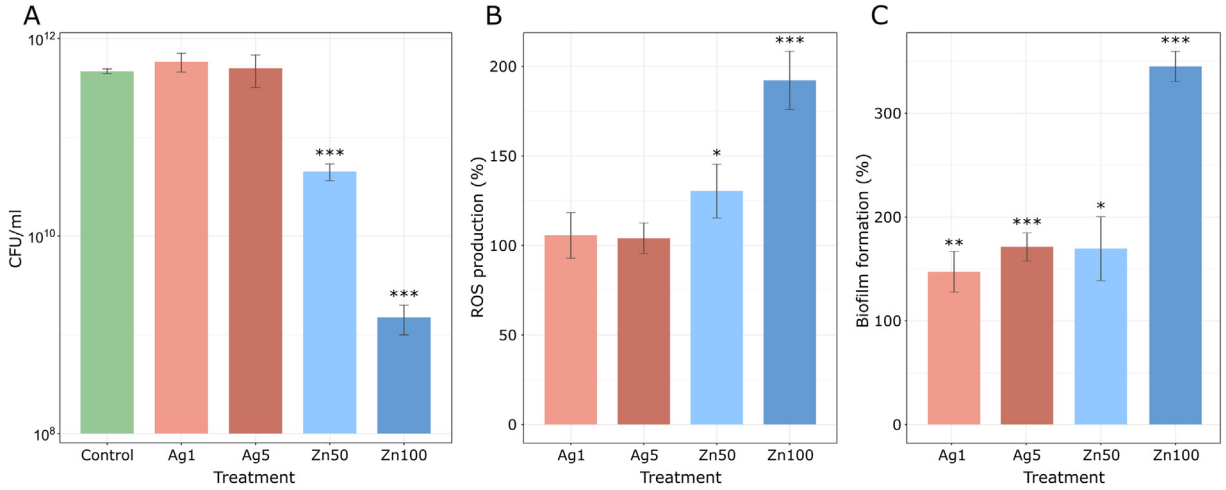


**Fig. 1.** Responses of *P. aeruginosa* to Ag and ZnO NPs exposition. A) Total cell count after 24 h incubation. B) Relative fluorescence production after DCFH staining, relative to control levels. C) Total biofilm biomass relative to control production, after 24 h incubation. Ag1 and Ag5 refers to Ag NPs at 1 and 5 mg/L, and Zn50 and Zn100 to ZnO NPs at 50 and 100 mg/L, respectively. Error bars refer to ± standard deviation from the mean of triplicate measurements.

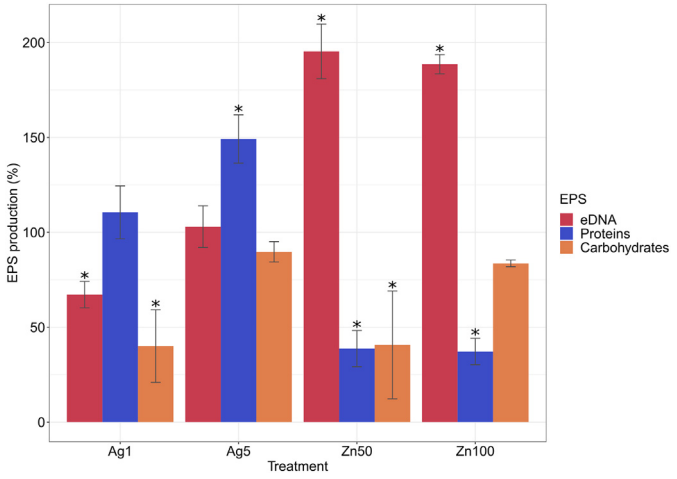


**Fig. 2.** Characterization of biofilms produced by *P. aeruginosa* exposed to Ag (1 and 5 mg/L) and ZnO (50 and 100 mg/L) NPs compared to unexposed control cultures. A) Amounts of eDNA (red bars), proteins (blue bars) and carbohydrates (orange bars) in the biofilm matrix of treated cultures, relative to untreated cultures. B) UV/vis spectra of biofilm matrix of treated and untreated samples diluted in saline buffer. Asterisks (*) represents significant differences compared to control samples ($p$-value <0.05). Error bars refer to ± standard deviation from the mean of triplicate measurements.

in the data obtained on this parameter. Bacteria secrete EPS in response to different stress agents, such as NPs at non-inhibitory concentrations (Chen et al., 2012). Biofilm formation and EPS production are important mechanisms for the bacterial resistance against heavy metals (Chien et al., 2013). The concentrations of Ag and ZnO NPs used in this work were not sufficient to completely inhibit cell growth and biofilm formation, thus the cells could recover growth and develop biofilms, as a response to the multiple stresses caused by NPs (Al-Shabib et al., 2016). Besides, subinhibitory concentrations of Ag NPs have been shown to enhance biofilm formation in *P. aeruginosa* isolates (Saeki et al., 2021). The best-known mechanims in *P. aeruginosa* for eDNA release are through cell death by production of $H_2O_2$ or pyocyanin, but also, ROS production can enhance this process (Sarkar, 2020). In fact, this is a plaussible explanation of our results, relating the increase in eDNA concentration in ZnO NPs treatment with the increase of intracellular ROS produced. Outer-membrane stresses triggered by oxidants, bactericides or, as in this study, metalic NPs, favor the EPS production (Riquelme et al., 2020). Although it increases the amount of eDNA released, cell death prevents the production and release of proteins or carbohydrates as protective EPS.

We compared the structure of biofilms formed under the studied conditions, using CLSM (Table 1). The control biofilm of *P. aeruginosa* M3.15R2 showed an average thickness of 23.16 ± 5.37 μm, with few dead cells (red) dispersed in between the live (green) cells (Fig. 3A). Ag NPs at 1 and 5 mg/L produced the same effect on *P. aeruginosa* biofilms. Biofilms treated with Ag NPs had no difference in cellular biomass when compared to control conditions, however, they were thinner and presented less surface area and roughness. The concentrations of Ag NPs tested caused some cell damage but, over time, cell growth recovered (Fig. S3), and the development of biofilms accelerated resulting in homogeneous biofilms (Fig. 3BC) (Ouyang et al., 2020). On the other hand, the studied ZnO NPs concentrations were more toxic than those of Ag NPs to *P. aeruginosa*. This resulted in less cellular biomass at 100 mg/L ZnO NPs compared with the control condition, although no significant differences in cellular biomass were found at 50 mg/L. Compared to control biofilms, the exposure to 100 mg/L ZnO NPs produced very heterogeneous biofilms, with a higher roughness coefficient (Table 1). ZnO NPs reduced the surface coverage and broke the microstructure of biofilms causing a rougher and patchier bacterial colonization of the slides (Moreno et al., 1993; Rodrigues and Elimelech, 2010). The increase in the number of living bacteria allowed an accelerated biofilm formation as response of the stress caused by ZnO NPs, and thus, producing a more complex biofilm than with 100 mg/L ZnO NPs (Fig. 3DE). The sensitivity of the confocal laser scanning microscope and the stains used were not appropriate for eDNA staining (Dominiak et al., 2011; Domenech et al., 2016), thus we could not observe the increase in eDNA release in presence of ZnO NPs.

### 3.3. Transcriptomic responses to ZnO and Ag NPs

We compared the transcriptomic responses of *P. aeruginosa* M3.15R2 strain after exposition to Ag NPs (1 and 5 mg/L) and ZnO NPs (50 and 100 mg/L) with that in control conditions. We observed conserved transcriptomic profiles of *P. aeruginosa* in response to the different metallic NPs studied, being more similar at different concentrations of the same NPs. Besides, the transcriptome of Ag NPs treated cultures were more similar to control than to ZnO NPs treated cultures (Fig. S4). We found 60 Differentially Expressed Genes (DEGs) in common between all the experimental conditions tested (Fig. 4A; Supplementary Table S3). ZnO NPs also produced bigger transcriptomic changes, with 753 and 934 DEGs ($|logFC| > 1$, $FDR < 0.05$), and an accumulated absolute fold change (log2) of 1395.86 and 1746.01 in presence of 50 mg/L and 100 mg/L, respectively. Meanwhile, Ag NPs produced smaller changes, with 135 and 270 DEGs, and 178.55 and 368.12 absolute accumulated fold change at 1 and 5 mg/L, respectively (Fig. 4B).

DEGs were mapped to the gene ontology (GO) database to elucidate enriched biological processes. After treating *P. aeruginosa* cultures with 50 and 100 mg/L ZnO NPs the transcriptomic responses were similar, having in common most of their enriched biological processes, which were mainly related to oxidation and reduction, biosynthesis, and transport. However, the processes enriched by Ag NPs treatment were related with the iron homeostasis and transport, being the later a conserved response to both Ag and ZnO NPs treatment (Fig. 4C).

Ag and ZnO NPs are described to induce the production of intracellular ROS and the expression of oxidative stress related genes (Dwivedi et al., 2014; Yan et al., 2018), however, we only observed the upregulation of *sodM* that encodes for a superoxide dismutase (SodA). While no impact in ROS production was observed under Ag NPs treatment, a significative increase was observed under ZnO NPs treatment (Fig. 1B), and accordingly, a downregulation of some genes related to oxidative stress response (Fig. 5; Supplementary Table S4). Additionally, under ZnO NPs treatment, we observed an increase in the expression levels of the *fprA* gene, which is involved in the release of stored iron, in ferritin-like molecules, into the

**Table 1**
COMSTAT analysis of biofilm development experiments[1].

| Treatment[2] | Roughness | Surface/biovolume ratio | Surface area | Biomass | Average thickness |
|---|---|---|---|---|---|
| Ag1 | 0.18 ± 0.02$^{c}$ | 1.70 ± 0.12$^{b}$ | 1.40 × $10^{6}$ ± 2.46 x $10^{5b}$ | 9.75 ± 1.47$^{a}$ | 11.29 ± 1.68$^{b}$ |
| Ag5 | 0.20 ± 0.07$^{c}$ | 1.96 ± 0.64$^{b}$ | 1.30 × $10^{6}$ ± 6.89 x $10^{4b}$ | 9.17 ± 0.99$^{a}$ | 11.10 ± 0.86$^{b}$ |
| Zn50 | 0.46 ± 0.20$^{b}$ | 1.83 ± 0.09$^{b}$ | 1.43 × $10^{6}$ ± 3.77 x $10^{5b}$ | 9.19 ± 2.24$^{a}$ | 11.70 ± 2.19$^{b}$ |
| Zn100 | 1.55 ± 0.21$^{a}$ | 4.11 ± 0.98$^{a}$ | 2.61 × $10^{5}$ ± 9.17 x $10^{4c}$ | 0.90 ± 0.60$^{b}$ | 4.72 ± 1.19$^{c}$ |
| Control | 0.45 ± 0.20$^{b}$ | 4.44 ± 0.52$^{a}$ | 3.09 × $10^{6}$ ± 5.74 x $10^{5a}$ | 7.98 ± 1.96$^{a}$ | 23.16 ± 5.37$^{a}$ |

ANOVA test and LSD test were performed (a, b and c indicate significance groups).
[1] Results are averages ± standard deviation for $n = 5$ samples.
[2] Ag1 and Ag5 refers to Ag NPs at 1 and 5 mg/L, and Zn50 and Zn100 to ZnO NPs at 50 and 100 mg/L, respectively.

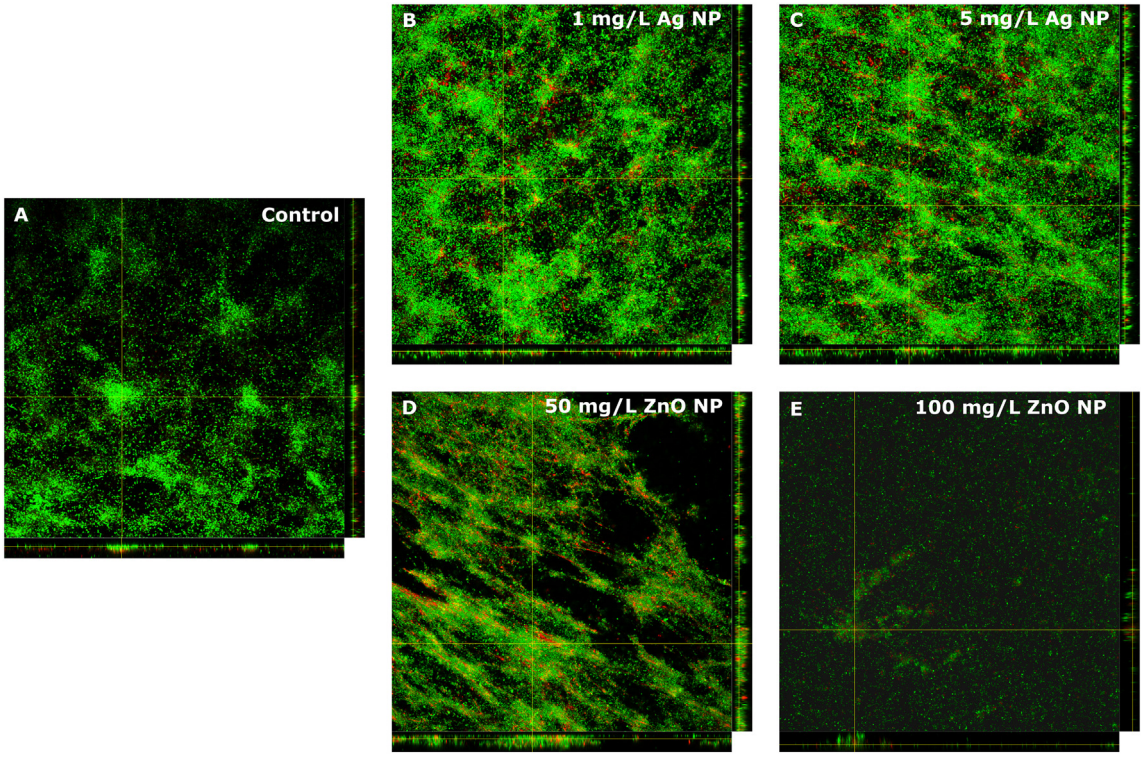


**Fig. 3.** Confocal laser scanning microscopy (CLSM) images of *P. aeruginosa* biofilms after 24 h incubation in A) absence of NPs, and in presence of B) 1 mg/L Ag NP, C) 5 mg/L Ag NPs, D) 50 mg/L ZnO NPs, and E) 100 mg/L ZnO NPs. Cells were stained using the LIVE/DEAD BacLight Bacterial Viability Kit with propidium iodide (PI) and SYTO9 to detect dead (red) and live (green) cells, respectively.

cytoplasm (Romsang et al., 2015). This excess of labile iron can create harmful side effects via the Fenton reaction, which leads to hydroxyl radicals (HO•) and ROS production (Morones-Ramirez et al., 2013). Besides, we observed the upregulation of *fprB* gene in every studied experimental condition, which is required for [4Fe4S] cluster biosynthesis, potentially causing a decrease of intracellular iron availability (Romsang et al., 2015). The higher intracellular ROS production under ZnO NPs treatment may be related to the imbalance of iron homeostasis in *P. aeruginosa* cells.

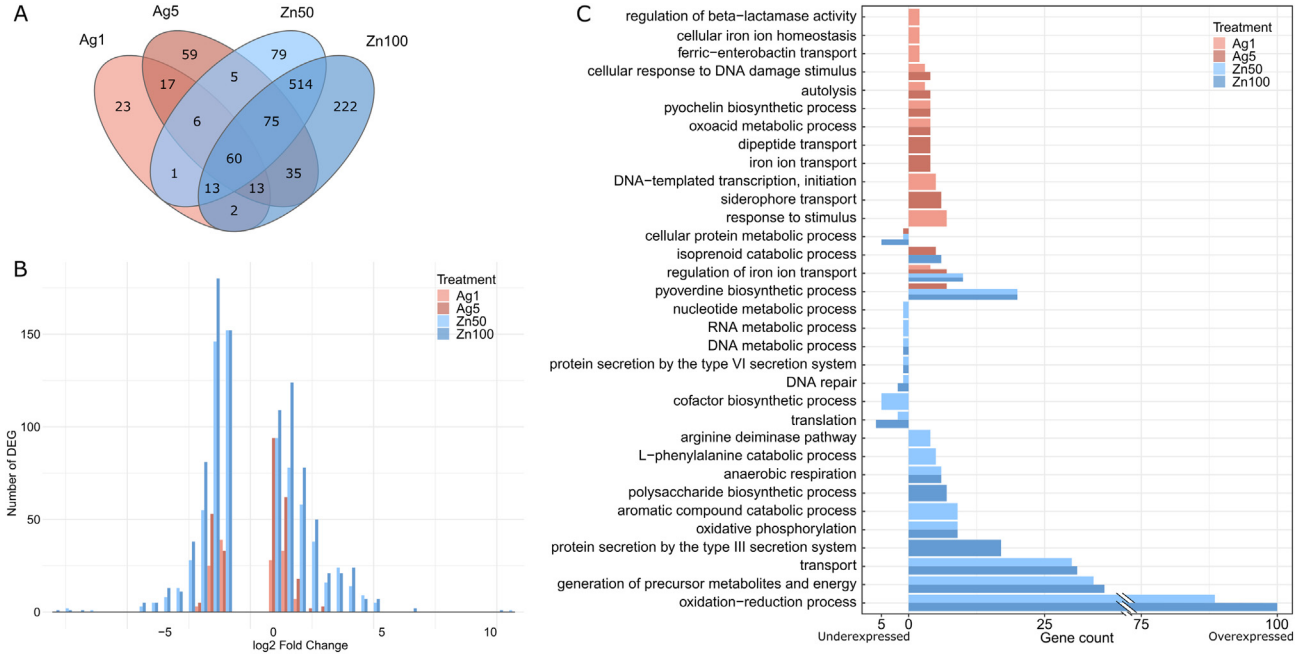


**Fig. 4.** Expression and function analysis of the transcriptome in Ag and ZnO NPs treated *P. aeruginosa*. Ag1 and Ag5 refers to Ag NPs at 1 and 5 mg/L, and Zn50 and Zn100 to ZnO NPs at 50 and 100 mg/L, respectively. A) Venn diagram representing the shared differentially expressed genes (DEG) between treatments. B) Histogram showing the log fold change frequency of the different conditions of Ag (red) and ZnO (blue) NPs. C) GO enrichment cluster analysis of the DEGs, representing the biological processes enriched.

Moreover, biological processes enriched by Ag and ZnO NPs are related to this iron homeostasis and transport, indicating the importance of such element in the response to the stress caused by said NPs. The iron imbalance may be justified by the upregulation of siderophore biosynthesis genes, pyochelin and pyoverdine (Takase et al., 2000). Iron is important for *P. aeruginosa* biofilm development, promoting the production of exopolysaccharides and reducing the synthesis of rhamnolipids (Yu et al., 2016). However, in addition to improving the bioavailability of iron, bacteria also use these siderophores to bind other metals and reduce the concentration of free toxic metals in the environment (Hesse et al., 2018; Sun et al., 2021). In Fig. 5 it can be observed the upregulation of said siderophores under Ag and ZnO NPs treatment. This siderophore overproduction can be the response of this WWTP adapted *P. aeruginosa* strain, explaining the differences in the described response mechanisms with clinical isolates (Zhang et al., 2020). Finally, we found that the transcripts of prrF1 and prrF2, which regulate several genes involved in protection from oxidative stress and iron storage (Reinhart et al., 2015), were overexpressed in presence of ZnO NPs. A potential adaptive mechanism has been described suggesting that regulatory PrrF sRNAs are key players mediating eDNA release leading to increased biofilm formation (Tahrioui et al., 2019). This would explain the increased eDNA concentration observed, which would shield biofilms against antimicrobial particles, such as ZnO NPs.

Concerning quorum sensing (QS), we observed a downregulation of *lasI* (acyl-homoserine lactone synthase) under ZnO NPs treatment. It has been reported an inhibition of QS processes by Ag and ZnO NPs in *P. aeruginosa* and other bacteria with similar QS systems (Gómez-Gómez et al., 2019a; Badawy et al., 2020). Besides, QS inhibition by heavy metal NPs is described to inhibit biofilm formation in *P. aeruginosa* by distortion of the biofilm structure (Gómez-Gómez et al., 2019b). However, we did not observe any significant and conserved change concerning QS, aside from the aforementioned repression of *lasI*. Apart from the ROS production, the increased eDNA release in presence of ZnO NPs could also be explained by an increase in QS regulated phenazine production (de Celis et al., 2021), however, we did not observe any significant changes in the phenazine

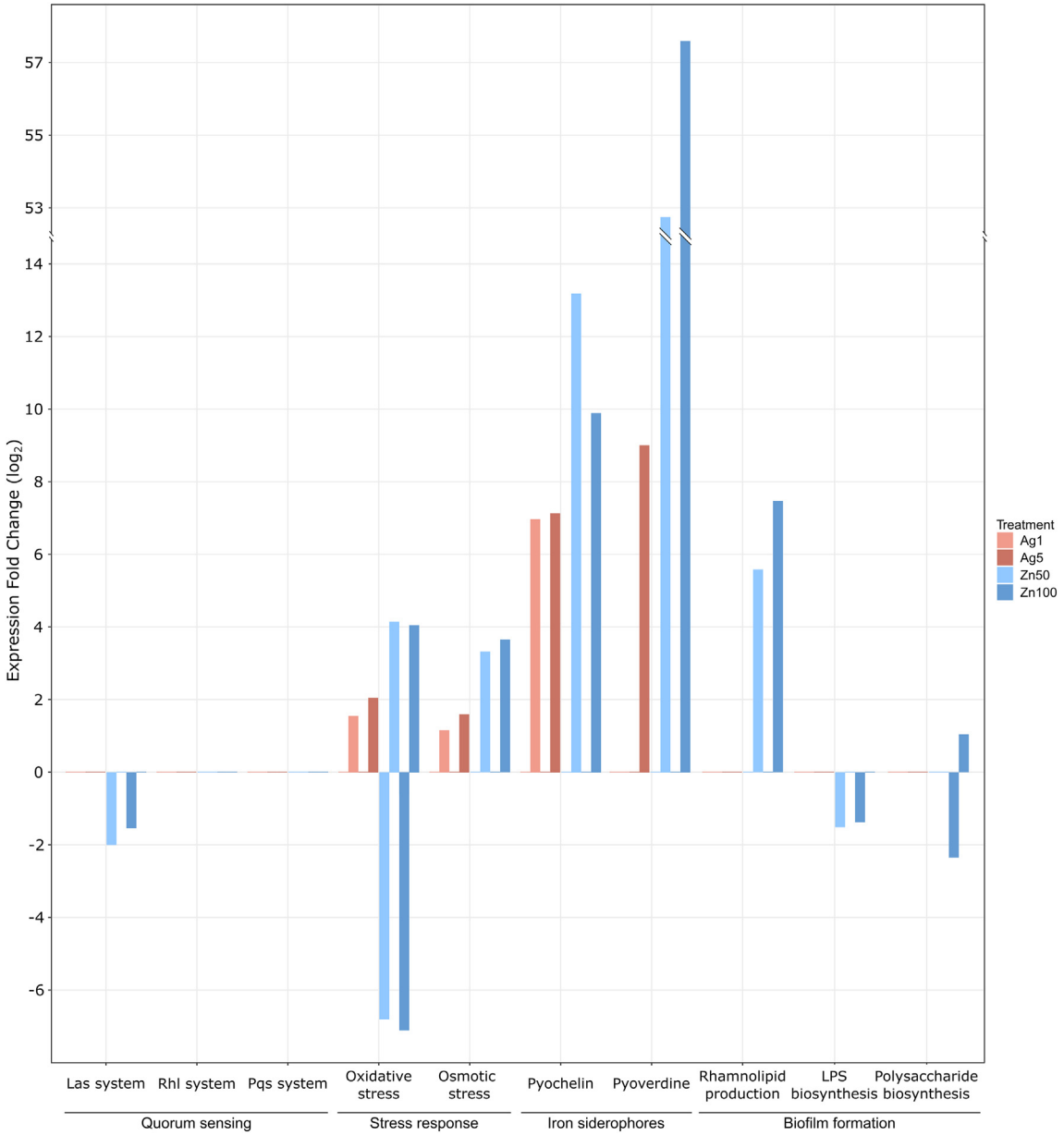


**Fig. 5.** Transcriptomic analysis of *P. aeruginosa* exposed to studied concentrations of Ag and ZnO NPs. Selected genes from functional categories of interest. Expression fold change is calculated against untreated cultures. Ag1 and Ag5 refers to Ag NPs at 1 and 5 mg/L, and Zn50 and Zn100 to ZnO NPs at 50 and 100 mg/L, respectively. All changes in gene expression are expressed as the fold change of the genes under the NP-treated condition compared to the untreated condition.

biosynthesis pathway. Interestingly, we observed an increase in biofilm formation, which is regulated, among other processes, by QS (Flemming et al., 2016). The expression of *rhlABC* rhamnolipid production genes were increased in the presence of ZnO NPs. Rhamnolipids play multiple roles in biofilm formation, like allowing surface motility, maintaining channel structures, or inducing biofilm dispersion (Rasamiravaka et al., 2015). In addition to QS regulation, rhamnolipid production is also induced by iron-limiting conditions, increasing surface motility and the formation of flat biofilms (Glick et al., 2010), like those observed under ZnO NPs treatment.

## 4. Conclusions

This work reports the adaptive response of a WWTP-isolated *P. aeruginosa* strain to Ag and ZnO NPs exposition. The transcriptomic and phenotypic responses of *P. aeruginosa* to Ag NPs were mainly related to the biofilm formation and iron homeostasis. The biofilms formed under Ag NPs treatment were on average thinner, and more homogeneous than control biofilms. During the growth, *P. aeruginosa* suffered the toxicity of Ag NPs, but could recover and the development of biofilms is accelerated in response to the stress, resulting in simple and homogeneous biofilms (lower roughness and surface to biovolume ratio). ZnO NPs also altered the biofilm formation and iron homeostasis in *P. aeruginosa* cells, however, the higher and more toxic concentrations utilized produced an increased cell death and eDNA release. Thus, the lower biofilm development was based on EPS production, via eDNA release. The transcriptomic response of *P. aeruginosa* to ZnO NPs was also higher compared to Ag NPs, with 5 to 10 times the accumulated fold change and differentially expressed genes. Both Ag and ZnO NPs are reported to cause cell death and disruption of QS and biofilm formation on clinical isolates of *P. aeruginosa.* However, we observed an increase in biofilm biomass, and cell death only by ZnO NPs, while expression of QS system genes remained unaltered. A possible explanation is that the studied strain is well adapted to wastewater conditions, where biofilm formation and siderophore production is increased as an adaptive mechanism to cope with high heavy metal concentrations (Sun et al., 2021). Although we found a conserved response of *P. aeruginosa* to the presence of the two studied metallic NPs (Fig. 4a), the higher and more toxic concentrations of ZnO NPs produced significant changes concerning cell viability and ROS production, leading to greater alterations on the transcriptome and biofilm structure.

In this work we report the possible adaptive mechanisms by which *P. aeruginosa* could survive potentially high environmental concentrations of metal-based nanoparticles. This study contributes to improve our understanding between biofilm and metal-based nanoparticles, giving a better insight in the effect of nanomaterials on biofilm formation in the natural environment. Potential releases of these nanoparticles might accelerate biofouling and biocorrosion in industrial systems or alter ecological balances in natural systems.

Supplementary data to this article can be found online at https://doi.org/10.1016/j.scitotenv.2022.153915.

## Data availability

Raw fastq files of the transcriptome analysis are available in the NCBI repository under the project code PRJNA770148.

## CRediT authorship contribution statement

I.B. D.M, and A.S. conceived the work. M.C., I.B. and A.S. designed the experimental and analytical approaches M.C., and I.B. performed the data analysis. M.C., I.B., D.M. and A.S. discussed the results. M.C., I.B. and A.S. wrote the manuscript.

## Declaration of competing interest

The authors declare no conflict of interest.

## Acknowledgements

This research was funded by the Spanish Ministry of Economy, Industry and Competitiveness, in the framework of the project CTM2016-76491-P. Miguel de Celis holds a PhD grant associated to this project (FPI grant: BES-2017-080024). Likewise, this work was supported by Ministry of Economy, Industry and Competitiveness of Spain, CTQ2014-60250-R project. The authors also want to thank Alicia Barroso and Eduardo A. León from the IPB López Neyra (CSIC) genomic and bioinformatic teams for their efforts in NGS analysis. We are also grateful to Dr. Yolanda Madrid and Beatriz Gómez-Gómez from the Department of Analytical Chemistry, Complutense University of Madrid for their contribution and advice with the use of nanoparticles.

## References

Ahmed, B., Solanki, B., Zaidi, A., Khan, M.S., Musarrat, J., 2019. Bacterial toxicity of biomimetic green zinc oxide nanoantibiotic: insights into ZnONP uptake and nanocolloid–bacteria interface. Toxicol. Res. 8, 246–261.

Al-Shabib, N., Husain, F., Ahmed, F., Khan, R.A., Ahmad, I., Alsharaeh, E., Khan, M.S., Hussain, A., Rehman, M.T., Yusuf, M., Hassan, I., Khan, J.M., Ashraf, G.M., Alsalme, A., Al-Ajmi, M.F., Tarasov, V.V., Aliev, G., 2016. Biogenic synthesis of zinc oxide nanostructures from Nigella sativa seed: prospective role as food packaging material inhibiting broad-spectrum quorum sensing and biofilm. Sci. Rep. 6, 36761.

Anders, S., Pyl, P.T., Huber, W., 2015. HTSeq—a Python framework to work with high-throughput sequencing data. Bioinformatics 31 (2), 166–169.

Andres-Leon, E., Nunez-Torres, R., Rojas, A.M., 2016. miARma-seq: a comprehensive tool for miRNA, mRNA and circRNA analysis. Sci. Rep. 6, 25749.

Andrews, S., 2010. FastQC: a quality control tool for high throughput sequence data. Available online at: http://www.bioinformatics.babraham.ac.uk/projects/fastqc.

Badawy, M.S.E.M., Riad, O.K.M., Taher, F.A., Zaki, S.A., 2020. Chitosan and chitosan-zinc oxide nano composite inhibit expression of LasI and RhlI genes and quorum sensing dependent virulence factors of Pseudomonas aeruginosa. Int. J. Biol. Macromol. 149, 1109–1117.

Beisl, S., Monteiro, S., Santos, R., Figueiredo, A.S., Sánchez-Loredo, M.G., Lemos, M.A., Lemos, F., Minhalma, M., de Pinho, M.N., 2019. Synthesis and bactericide activity of nanofiltration composite membranes – cellulose acetate/silver nanoparticles and cellulose acetate/silver ion exchanged zeolites. Water Res. 149, 225–231.

Brar, S.K., Verma, M., Tyagi, R.D., Surampalli, R.Y., 2010. Engineered nanoparticles in wastewater and wastewater sludge – evidence and impacts. Waste Manag. 30 (3), 504–520.

de Celis, M., Belda, I., Ortiz-Álvarez, R., Arregui, L., Marquina, D., Serrano, S., Santos, S., 2020. Tuning up microbiome analysis to monitor WWTPs' biological reactors functioning. Sci. Rep. 10, 4079.

de Celis, M., Serrano-Aguirre, L., Belda, I., Liébana-García, R., Arroyo, M., Marquina, D., de la Mata, I., Santos, A., 2021. Acylase enzymes disrupting quorum sensing alter the transcriptome and phenotype of Pseudomonas aeruginosa, and the composition of bacterial biofilms from wastewater treatment plants. Sci. Total Environ. 799, 149401.

Chen, P.Y., Powell, B.A., Mortimer, M., Ke, P.C., 2012. Adaptive interactions between zinc oxide nanoparticles and Chlorella sp. Environ. Sci. Technol. 46, 12178–12185.

Chen, Q., Li, T., Gui, M., Liu, S., Zheng, M., Ni, J., 2017. Effects of ZnO nanoparticles on aerobic denitrification by strain Pseudomonas stutzeri PCN-1. Bioresour. Technol. 239, 21–27.

Chien, C.C., Lin, B.C., Wu, C.H., 2013. Biofilm formation and heavy metal resistance by an environmental Pseudomonas sp. Biochem. Eng. J. 78, 132–137.

Danabas, D., Ates, M., Ertit Tastan, B., Cicek Cimen, I.C., Unal, I., Aksu, O., Kutlu, B., 2020. Effects of Zn and ZnO nanoparticles on Artemia salina and Daphnia manga organisms: toxicity, accumulation, and elimination. Sci. Total Environ. 711, 134869–134878.

Dhas, S.P., Shiny, P.J., Khan, S.S., Mukherjee, A., Chandrasekaran, N., 2013. Toxic behavior of silver and zinc oxide nanoparticles on environmental microorganisms. J. Basic Microbiol. 4, 916–927.

Domenech, M., Pedrero-Vega, E., Prieto, A., García, E., 2016. Evidence of the presence of nucleic acids and β-glucan in the matrix of non-typeable Haemophilus influenzae in vitro biofilms. Sci. Rep. 6, 36424.

Dominiak, D.M., Nielsen, J.L., Nielsen, P.H., 2011. Extracellular DNA is abundant and important for microcolony strength in mixed microbial biofilms. Environ. Microbiol. 13, 710–721.

Dubois, M., Gilles, K.A., Hamilton, J.K., Rebers, P.A., Smith, F., 1956. Colorimetric method for determination of sugars and related substances. Anal. Chem. 28, 350–356.

Durenkamp, M., Pawlett, M., Ritz, K., Harris, J.A., Neal, A.L., McGrath, S.P., 2016. Nanoparticles within WWTP sludges have minimal impact on leachate quality and soil microbial community structure and function. Environ. Pollut. 211, 399–405.

Dwivedi, S., Wahab, R., Khan, F., Mishra, Y.K., Musarrat, J., Al-Khedhairy, A.A., 2014. Reactive oxygen species mediated bacterial biofilm inhibition via zinc oxide nanoparticles and their statistical determination. PLoS ONE 9, e111289.

Fabrega, J., Louma, S.N., Tyler, C.R., Galloway, T.S., Lead, J.R., 2011. Silver nanoparticles: behaviour and effects in the aquatic environment. Environ. Int. 37, 517–531.

Fauss, E.K., MacCuspie, R.I., Oyanedel-Craver, V., Smith, J.A., Swami, N.S., 2014. Disinfection action of electrostatic versus steric-stabilized silver nanoparticles on E. coli under different water chemistries. Colloids Surf. B Biointerfaces 113, 77–84.

Flemming, H.C., Wingender, J., 2010. The biofilm matrix. Nat. Rev. Microbiol. 8, 623–633.

Flemming, H.C., Wingender, J., Kjelleberg, S., Steinberg, P., Rice, S., Szewzyk, U., 2016. Biofilms: an emergent form of bacterial life. Nat. Rev. Microbiol. 14, 563–575.

Gerber, I.B., Dubery, I.A., 2003. Fluorescence microplate assay for the detection of oxidative burst products in tobacco cell suspensions using 2',7'-dichloro-fluorescein. Methods Cell Sci. 25, 115–122.
Glick, R., Gilmour, C., Tremblay, J., Satanower, S., Avidan, O., Deziel, E., Greenberg, E.P., Poole, K., Banin, E., 2010. Increase in rhamnolipid synthesis under iron-limiting conditions influences surface motility and biofilm formation in Pseudomonas aeruginosa. J. Bacteriol. 192, 2973–2980.
Gómez-Gómez, B., Arregui, L., Serrano, S., Santos, A., Pérez-Corona, T., Madrid, Y., 2019a. Unravelling mechanisms of bacterial quorum sensing disruption by metal-based nanoparticles. Sci. Total Environ. 696, 133869.
Gómez-Gómez, B., Arregui, L., Serrano, S., Santos, A., Perez-Corona, M.T., Madrid, Y., 2019b. Selenium and tellurium-based nanoparticles as interfering factors on Quorum sensing-regulated processes: violacein production and bacterial biofilm formation. Metallomics 11, 1104–1114.
Gottschalk, F., Sonderer, T., Scholz, R.W., Nowack, B., 2009. Modelled environmental concentrations of engineered nanomaterials (TiO2, ZnO, Ag, CNT, fullerenes) for different regions. Environ. Sci. Technol. 43, 9216–9222.
Gottschalk, F., Sun, T., Nowack, B., 2013. Environmental concentrations of engineered nanomaterials: review of modeling and analytical studies. Environ. Pollut. 181, 287–300.
Guo, Z., Zhang, P., Luo, Y., Xie, H.Q., Chakraborty, S., Monikh, F.A., Bu, L., Liu, Y., Ma, Y., Zhang, Z., Valsami-Jones, E., Zhao, B., Lynch, I., 2020. Intranasal exposure to ZnO nanoparticles induces alterations in cholinergic neurotransmission in rat brain. Nano Today 35, 100977.
Gwin, C.A., Lefevre, E., Alito, C.L., Gunsch, C.K., 2018. Microbial community response to silver nanoparticles and Ag+ in nitrifying activated sludge revealed by ion semiconductor sequencing. Sci. Total Environ. 616–617, 1014–1021.
Habash, M.B., Goodyear, M.C., Park, A.J., Surette, M.D., Vis, E.C., Harris, R.J., Khursigara, C.M., 2017. Potentiation of tobramycin by silver nanoparticles against Pseudomonas aeruginosa biofilms. Antimicrob. Agents Chemother. 61, e00415–e00417.
Hesse, E., O'Brien, S., Tromas, N., Bayer, F., Luján, A.M., van Veen, E.M., Hodgson, D.J., Buckling, A., 2018. Ecological selection of siderophore-producing microbial taxa in response to heavy metal contamination. Ecol. Lett. 21, 117–127.
Heydorn, A., Nielsen, A.T., Hentzer, M., Sternberg, C., Givskov, M., Ersbøll, B.K., Mølin, S., 2000. Quantification of biofilm structures by the novel computer program COMSTAT. Microbiology-UK 146, 2395–2407.
Hotze, E.M., Phenrat, T., Lowry, G.V., 2010. Nanoparticle aggregation: challenge to understanding transport and reactivity in the environment. J. Environ. Qual. 39 (6), 1909–1924.
Huang, H., Peng, C., Peng, P., Lin, Y., Zhang, X., Ren, H., 2019. Towards the biofilm characterization and regulation in biological wastewater treatment. Appl. Microbiol. Biotechnol. 103 (3), 1115–1129.
Ivask, A., Juganson, K., Bondarenko, O., Mortimer, M., Aruoja, V., Kasemets, K., Blinova, I., Heinlaan, M., Slaveykova, V., Kahru, A., 2014. Mechanisms of toxic action of Ag, ZnO and CuO nanoparticles to selected ecotoxicological test organisms and mammalian cells in vitro: a comparative review. Nanotoxicology 8, 57–71.
Jennings, L.K., Storek, K.M., Ledvina, H.E., Coulon, C., Marmont, L.S., Sadovskaya, I., Secor, P.R., Tseng, B.S., Scian, M., Filloux, A., Wozniak, D.J., Howell, P.L., Parsek, M.R., 2015. Pel is a cationic exopolysaccharide that cross-links extracellular DNA in the Pseudomonas aeruginosa biofilm matrix. Proc. Natl. Acad. Sci. U. S. A. 112 (36), 11353–11358.
Jones, N., Ray, B., Ranjit, K.T., Manna, A.C., 2008. Antibacterial activity of ZnO nanoparticle suspensions on a broad spectrum of microorganisms. FEMS Microbiol. Lett. 279, 71–76.
Klausen, M., Heydorn, A., Ragas, P., Lambertsen, L., Aaes-Jørgensen, A., Molin, S., Tolker-Nielsen, T., 2003. Biofilm formation by Pseudomonas aeruginosa wild type, flagella and type IV pili mutants. Mol. Microbiol. 48, 1511–1524.
Kopylova, E., Noe, L., Touzet, H., 2012. SortMeRNA: fast and accurate filtering of ribosomal RNAs in metatranscriptomic data. Bioinformatics 28, 3211–3217.
Lalley, J., Dionysiou, D.D., Varma, R.S., Shankara, S., Yang, D.J., Nadagouda, M.N., 2014. Silver-based antibacterial surfaces for drinking water disinfection - an overview. Curr. Opin. Chem. Eng. 3, 25–29.
Li, H., Durbin, R., 2009. Fast and accurate short read alignment with burrows-wheeler transform. Bioinformatics 25, 1754–1760.
Li, L., Stoiber, M., Wimmer, A., Xu, Z., Lindenblatt, C., Helmreich, B., Schuster, M., 2016. To what extent can full-scale wastewater treatment plant effluent influence the occurrence of silver-based nanoparticles in surface waters? Environ. Sci. Technol. 50 (12), 6327–6333.
Liao, S., Zhang, Y., Pan, X., Zhu, F., Jiang, C., Liu, Q., Cheng, Z., Dai, G., Wu, G., Whang, L., Chen, L., 2019. Antibacterial activity and mechanism of silver nanoparticles against multidrug-resistant Pseudomonas aeruginosa. Int. J. Nanomedicine 14, 1469–1487.
Liu, C., Faria, A.F., Ma, J., Elimelech, M., 2017. Mitigation of biofilm development on thin-film composite membranes functionalized with zwitterionic polymers and silver nanoparticles. Environ. Sci. Technol. 51, 182–191.
Love, M.I., Huber, W., Anders, S., 2014. Moderated estimation of fold change and dispersion for RNA-seq data with DESeq2. Genome Biol. 15, 550.
Ma, H.B., Williams, P.L., Diamond, S.A., 2013. Ecotoxicity of manufactured ZnO nanoparticles - a review. Environ. Pollut. 172, 76–85.
Majedi, S.M., Lee, H.K., Kelly, B.C., 2012. Chemometric analytical approach for the cloud point extraction and inductively coupled plasma mass spectrometric determination of zinc oxide nanoparticles in water samples. Anal. Chem. 84, 6546–6552.
Merritt, J.H., Kadouri, D.E., O'Toole, G.A., 2005. Growing and analyzing static biofilms. Curr. Protoc. Microbiol. Chapter 1, Unit 1B.1.
Moreno, D.A., Ibars, J.R., Beech, I.B., Gaylarde, C.C., 1993. Biofilm formation on mild steel coupons by Pseudomonas and Desulfovibrio. Biofouling 7, 129–139.
Morones-Ramirez, J.R., Winkler, J.A., Spina, C.S., Collins, J.J., 2013. Silver enhances antibiotic activity against gram-negative bacteria. Sci. Transl. Med. 5, 190ra81.
Nanocomposix, x. 20 nm Silver Nanospheres, Citrate, NanoXact™. Retrieved December 28, 2021, from https://tools.nanocomposix.com:48/cdn/coa/Silver/Spheres/NanoXact/AG20-NX-CIT-SS-ECP1559.pdf?1241452.
Ouyang, K., Mortimer, M., Holden, P.A., Cai, P., Wu, Y., Gao, C., Huang, Q., 2020. Towards a better understanding of Pseudomonas putida biofilm formation in the presence of ZnO nanoparticles (NPs): role of NP concentration. Environ. Int. 137, 105485.
Pati, R., Mehta, R.K., Mohanty, S., Padhi, A., Sengupta, M., Vaseeharan, B., Goswami, C., Sonawane, A., 2014. Topical application of zinc oxide nanoparticles reduces bacterial skin infection in mice and exhibits antibacterial activity by inducing oxidative stress response and cell membrane disintegration in macrophages. Nanomed. Nanotechnol. Biol. Med. 10, 1195–1208.
Periasamy, S., Nair, H.A.S., Lee, K.W.K., Ong, J., Goh, J.Q.J., Kjelleberg, S., Rice, S.A., 2015. Pseudomonas aeruginosa PAO1 exopolysaccharides are important for mixed species biofilm community development and stress tolerance. Front. Microbiol. 6, 851.
Pestrak, M.J., Chaney, S.B., Eggleston, H.C., Dellos-Nolan, S., Dixit, S., Mathew-Steiner, S.S., Roy, S., Parsek, M.R., Sen, C.K., Wozniak, D.J., 2018. Pseudomonas aeruginosa rugose small-colony variants evade host clearance, are hyper-inflammatory, and persist in multiple host environments. PLoS Pathog. 14 (2), e1006842.
Petzoldt, T., 2017. Estimation of growth rates with package growthrates. 1–8. Available at: https://cran.r-project.org/web/packages/growthrates/vignettes/Introduction.html.
Rasamiravaka, T., Labtani, Q., Duez, P., El Jaziri, M., 2015. The formation of biofilms by Pseudomonas aeruginosa: a review of the natural and synthetic compounds interfering with control mechanisms. Biomed. Res. Int. 2015, 759348.
Reinhart, A.A., Powell, D.A., Nguyen, A.T., O'Neill, M., Djapgne, L., Wilks, A., Ernst, R.K., Oglesby-Sherrouse, A.G., 2015. The prrF-encoded small regulatory RNAs are required for iron homeostasis and virulence of Pseudomonas aeruginosa. Infect. Immun. 83, 863–875.
Riquelme, S.A., Liimatta, K., Lung, T.W.F., Fields, B., Ahn, D., Chen, D., Lozano, C., Sáenz, Y., Uhlemann, A.C., Kahl, B.C., Britto, C.J., DiMango, E., Prince, A., 2020. Pseudomonas aeruginosa utilizes host-derived itaconate to redirect its metabolism to promote biofilm formation. Cell Metab. 31 (6), 1091–1106.e6.
Rodrigues, D.F., Elimelech, M., 2010. Toxic effects of single-walled carbon nanotubes in the development of E. coli biofilm. Environ. Sci. Technol. 44, 4583–4589.
Romsang, A., Duang-nkern, J., Wirathorn, W., Vattanaviboon, P., Mongkolsuk, S., 2015. Pseudomonas aeruginosa IscR-regulated ferredoxin NADP(+) reductase gene (fprB) functions in iron-sulfur cluster biogenesis and multiple stress response. PLoS ONE 10, e0134374.
Saeki, E.K., Yamada, A.Y., de Araujo, L.A., Anversa, L., Garcia, D.dO., de Souza, R.L.B., Martins, H.M., Kobayashi, R.K.T., Nakazato, G., 2021. Subinhibitory concentrations of biogenic silver nanoparticles affect motility and biofilm formation in Pseudomonas aeruginosa. Front. Cell. Infect. Microbiol. 11, 656984.
Sarkar, S., 2020. Release mechanisms and molecular interactions of Pseudomonas aeruginosa extracellular DNA. Appl. Microbiol. Biotechnol. 104, 6549–6564.
Sharma, G., Rao, S., Bansal, A., Dang, S., Gupta, S., Gabrani, R., 2014. Pseudomonas aeruginosa biofilm: potential therapeutic targets. Biologicals 42 (1), 1–7.
Sikder, M., Lead, J.R., Chandler, G.T., Baalousha, M., 2017. A rapid approach for measuring silver nanoparticle concentration and dissolution in sea water by UV-Vis. Sci. Total Environ. 618, 597–607.
Silva, T., Pokhrel, L.R., Dubey, B., Tolaymat, T.M., Maier, K.J., Liu, X., 2014. Particle size, surface charge and concentration dependent ecotoxicity of three organo-coated silver nanoparticles: comparison between general linear model-predicted and observed toxicity. Sci. Total Environ. 468–469 (15), 968–976.
da Silva, B.L., Abucafy, M.P., Manaia, E.B., Junior, J.A.O., Chiari-Andreo, B.G., Pietro, R.C.L., Chiavacci, L.P., 2019. Relationship between structure and antimicrobial activity of zinc oxide nanoparticles: an overview. Int. J. Nanomed. 14, 9395–9410.
Slavin, Y.N., Asnis, J., Hafeli, U.O., Bach, H., 2017. Metal nanoparticles: understanding the mechanisms behind antibacterial activity. J. Nanobiotechnol. 15, 65.
Slekovec, C., Plantin, J., Cholley, P., Thouverez, M., Talon, D., Bertrand, X., Hocquet, D., 2012. Tracking down antibiotic-resistant Pseudomonas aeruginosa isolates in a wastewater network. PLoS ONE 7, e49300.
Sun, T.Y., Bornhöft, N.A., Hungerbühler, K., Nowack, B., 2016. Dynamic probabilistic modeling of environmental emissions of engineered nanomaterials. Environ. Sci. Technol. 50 (9), 4701–4711.
Sun, Y., Wang, S., Liu, X., He, Y., Wu, H., Xie, W., Li, N., Hou, W., Dong, H., 2021. Iron availability is a key factor for freshwater cyanobacterial survival against saline stress. Environ. Res. 194, 110592.
Tahrioui, A., Duchesne, R., Bouffartigues, E., Rodrigues, S., Maillot, O., Tortuel, D., Hardouin, J., Taupin, L., Groleau, M.C., Dufour, A., Déziel, E., Brenner-Weiss, G., Feuilloley, M., Orange, N., Lesouhaitier, O., Cornelis, P., Chevalier, S., 2019. Extracellular DNA release, quorum sensing, and PrrF1/F2 small RNAs are key players in Pseudomonas aeruginosa tobramycin-enhanced biofilm formation. npj Biofilms Microbiomes 5, 15.
Takase, H., Nitanai, H., Hoshino, K., Otani, T., 2000. Impact of siderophore production on Pseudomonas aeruginosa infections in immunosuppressed mice. Infect. Immun. 68, 1834–1839.
Tashiro, Y., Ichikawa, S., Shimizu, M., Toyofuku, M., Takaya, N., Nakajima-Kambe, T., Uchiyama, H., Nomura, N., 2010. Variation of physiochemical properties and cell association activity of membrane vesicles with growth phase in Pseudomonas aeruginosa. Appl. Environ. Microbiol. 76, 3732–3739.
Vestby, L.K., Grønseth, T., Simm, R., Nesse, L.L., 2020. Bacterial biofilm and its role in the pathogenesis of disease. Antibiotics 9 (2), 59.
West, S.A., Griffin, A.S., Gardner, A., Diggle, S.P., 2006. Social evolution theory for microorganisms. Nat. Rev. Microbiol. 4, 597–607.
Wimmer, A., Markus, A.A., Schuster, M., 2019. Silver nanoparticle levels in river water: real environmental measurements and modeling approaches—a comparative study. Environ. Sci. Technol. Lett. 6 (6), 353–358.
Yan, X., He, B., Liu, L., Qu, G., Shi, J., Hu, L., Jiang, G., 2018. Antibacterial mechanism of silver nanoparticles in Pseudomonas aeruginosa: proteomics approach. Metallomics 10, 557.
Yu, S., Wei, Q., Zhao, T., Guo, Y., Ma, L.Z., 2016. A survival strategy for Pseudomonas aeruginosa that uses exopolysaccharides to sequester and store iron to stimulate Psl-dependent biofilm formation. Appl. Environ. Microbiol. 82, 6403–6413.

Zhang, W., Yao, Y., Sullivan, N., Chen, Y., 2011. Modeling the primary size effects of citrate-coated silver nanoparticles on their ion release kinetics. Environ. Sci. Technol. 45, 4422–4428.

Zhang, Y., Pan, X., Liao, S., Jiang, C., Wang, L., Tang, Y., Wu, G., Dai, G., Chen, L., 2020. Quantitative proteomics reveals the mechanism of silver nanoparticles against multidrug-resistant Pseudomonas aeruginosa biofilms. J. Proteome Res. 19, 3109–3122.

Zhao, J., Lin, M., Wang, Z., Cao, X., Xing, B., 2021. Engineered nanomaterials in the environment: are they safe? Crit. Rev. Environ. Sci. Technol. 51 (14), 1443–1478.

Zwietering, M.H., Jongenburger, I., Rombouts, F.M., Van't Riet, K., 1990. Modeling of the bacterial growth curve. Appl. Environ. Microbiol. 56, 1875–1881.